Makara Journal of Science

Volume 26
Issue 3 *September*

Article 5

9-30-2022

# Comparative Study of Bismuth Ferrite Deposition Method on TiO2 Nanotube and Performance of Hydrogen Evolution in a Photoelectrochemical Dye-Sensitized Solar Cell Tandem System

Yunita Yunita
*Department of Chemistry, Faculty of Mathematics and Natural Sciences, Universitas Indonesia, Depok 16424, Indonesia*, yunitaid98@gmail.com

Muhammad Iqbal Syauqi
*Department of Chemistry, Faculty of Mathematics and Natural Sciences, Universitas Indonesia, Depok 16424, Indonesia*

Jarnuzi Gunlazuardi
*Department of Chemistry, Faculty of Mathematics and Natural Sciences, Universitas Indonesia, Depok 16424, Indonesia*



## Recommended Citation

Yunita, Yunita; Syauqi, Muhammad Iqbal; and Gunlazuardi, Jarnuzi (2022) "Comparative Study of Bismuth Ferrite Deposition Method on TiO2 Nanotube and Performance of Hydrogen Evolution in a Photoelectrochemical Dye-Sensitized Solar Cell Tandem System," *Makara Journal of Science*: Vol. 26: Iss. 3, Article 5.
DOI: 10.7454/mss.v26i3.1387
Available at: https://scholarhub.ui.ac.id/science/vol26/iss3/5

Makara Journal of Science, 26/3 (2022), 190–199
doi: 10.7454/mss.v26i3.1387

# Comparative Study of Bismuth Ferrite Deposition Method on $TiO_2$ Nanotube and Performance of Hydrogen Evolution in a Photoelectrochemical Dye-Sensitized Solar Cell Tandem System

Yunita*, Muhammad Iqbal Syauqi, and Jarnuzi Gunlazuardi

Department of Chemistry, Faculty of Mathematics and Natural Sciences, Universitas Indonesia, Depok 16424, Indonesia

*E-mail: yunitaid98@gmail.com

Received July 18, 2022 | Accepted September 21, 2022

## Abstract

Hydrogen is a renewable and environmentally friendly energy source that can replace fossil fuels by utilizing solar energy through water splitting. The hydrogen production was conducted in this research by using a tandem system of dye-sensitized solar cell–photoelectrochemical cell (DSSC–PEC) and a $TiO_2$ nanotube coated with $BiFeO_3$ ($BiFeO_3$/TNT) as a photoanode in the PEC. The deposition of $BiFeO_3$ on TNT was prepared using the following three methods: successive ionic layer adsorption and reaction (SILAR), ultrasonication-assisted SILAR, and ultrasonic– immersion method by varying the number of deposition cycles in each method. In this study, the optimum cycles for SILAR, ultrasonication-assisted SILAR, and ultrasonic–immersion methods were 15, 5, and 3, respectively. Results show that the $BiFeO_3$ deposited on TNT using the ultrasonic–immersion method with three cycles ($BiFeO_3$/TNT_UI3) demonstrates the best photoelectrochemical activity. The tandem system comprises $BiFeO_3$/TNT_UI3 photoanode and Pt-coated TNT dark cathode PEC cell connected to TNT/N719-based DSSC with an efficiency of 1.27%. The constructed DSSC–PEC system could produce $3.11 \times 10^{-6}$ mol hydrogen in 6 h with a solar-to-hydrogen (STH) efficiency of 0.0033% in an H-type reactor filled with 0.5 M $H_2SO_4$ electrolyte.

*Keywords: $BiFeO_3$/TNT, DSSC–PEC, hydrogen production*

## Introduction

Along with the times and the increasing human population, energy consumption continuously rises to meet the sustainability of human activities. Approximately 90% of the total energy use in the world is fossil fuels, which have remarkably limited availability and a negative impact on the environment, such as global warming and air pollution. These limitations and negative impacts encouraged researchers to turn to alternative environmentally friendly energy sources [1].

Hydrogen ($H_2$) is an alternative environmentally friendly energy source with high energy density per mass and energy efficiency [2]. Instead of steam reforming of methane gas from fossil fuels, several methods, such as photoelectrochemical, photobiological, photoelectrolysis, and photocatalytic approaches, can be used in hydrogen production [3, 4]. The photoelectrochemical method (photoelectrochemical cell, PEC) can efficiently produce hydrogen by utilizing semiconductors, light, and water because it is cost-effective and has high energy conversion efficiency [5]. The PEC method for hydrogen products was first reported by Fujishima and Honda in 1972 using a $TiO_2$ photoelectrode on PEC [6]. $TiO_2$ is a semiconductor characterized by its wide band gap (3.0–3.2 eV), good chemical stability, low cost, non-toxicity, corrosion resistance, and high photocatalytic activity [7]. However, the wide band gap of $TiO_2$ can only absorb ultraviolet (UV) light and is limited to absorbing visible light.

One way of modifying the $TiO_2$ semiconductor is by adding bismuth ferrite ($BiFeO_3$), which has a band gap of 2.0–2.8 eV; therefore, it can utilize visible light efficiently [8]. $BiFeO_3$ has non-toxic properties and good stability [9]. In addition, Liao *et al.* reported that the $BiFeO_3$/$TiO_2$ nanotube ($BiFeO_3$/TNT) heterojunction could increase the specific surface area, improve charge separation and electron–hole pair transfer efficiency, and inhibit their recombination. The activity of the $BiFeO_3$/TNT heterojunction was tested for the degradation of methylene blue within 180 min of 78.4% (UV) and 90.4% (visible light) [10]. A similar study was also conducted by Wu *et al*., where the deposition of $BiFeO_3$ on $TiO_2$ through five repetitions of the spin coating increased the current density by nearly 35 times than that of pure $TiO_2$ under

visible light illumination [11]. Zhao *et al*. synthesized $BiFeO_3$/TNT using an ultrasound-assisted SILAR method. The electrodes of $BiFeO_3$/TNT showed a surface photovoltage response twice as strong as that of TNT and increased photo electrocatalytic performance in the degradation of methylene blue up to 75.7% [12]. However, a single PEC cell of $BiFeO_3$/TNT is still insufficient in the water-splitting application due to the need for additional voltage bias to oxidize water.

A tandem system integrating DSSC and PEC cells can improve visible light harvesting by employing molecular photosensitizers on the surface of the oxide semiconductor. The additional energy provided by the DSSC can also eliminate the need for additional bias to split water into the conventional PEC cells [3]. Several studies have been conducted to develop a DSSC–PEC tandem system; for example, Samsudin *et al*. developed a DSSC–PEC tandem in series using $TiO_2$/$BiVO_4$ to produce hydrogen. They showed that $TiO_2$/$BiVO_4$ 0.8% wt succeeded in producing 692 umols of hydrogen in 120 min [13]. Surahman also developed a quantum dot sensitized solar cell-photoelectrochemical (QDSSC–PEC) tandem system for hydrogen production using a photocatalyst of TNT sensitized to CdS nanoparticles as electrodes in QDSSC and Pt/TNT as a cathode, which plays a role in reducing $H^+$ to $H_2$. The efficiency of hydrogen production through water splitting using CdS/TNT was 4.78% [14].

However, the authors believe that the use of BiFeO/TNT electrodes in the DSSC–PEC tandem system for $H_2$ evolution has not been previously reported. Therefore, hydrogen production was conducted by developing a DSSC–PEC tandem system using $BiFeO_3$/$TiO_2$ nanotube ($BiFeO_3$/TNT). The $BiFeO_3$/TNT was initially optimized by comparing the following three synthesis methods: SILAR, ultrasonication-assisted SILAR, and ultrasonic–immersion. The PEC cell comprises a photoanode ($BiFeO_3$/TNT) and a cathode (Pt/TNT) separated into a Nafion membrane in an H-type reactor. Meanwhile, the DSSC cell used TNT/N719 as an anode, electrolyte $I^-/I_3^-$, and Pt/FTO as a cathode.

## Materials and Methods

**Materials.** The materials used included the following: deionized water ($H_2O$), ammonium fluoride ($NH_4F$), dihexachloroplatinic (IV) acid ($H_2PtCl_6$), sulfuric acid ($H_2SO_4$), acetylacetone ($C_5H_8O_2$), acetone ($C_3H_6O$), acetonitrile ($CH_3CN$), iron (III) nitrate nonahydrate ($Fe(NO_3)_3.9H_2O$), bismuth (III) nitrate pentahydrate ($Bi(NO_3)_3.5H_2O$), ethanol ($C_2H_5OH$), ethylene glycol ($C_2H_6O_2$), fluorine-doped tin oxide (FTO) glass, iodine ($I_2$), potassium hydroxide (KOH), potassium iodide (KI), Nafion membrane, sodium sulfate ($Na_2SO_4$), and titanium (Ti) plate. All materials were obtained from Sigma-Aldrich and used as is, except for titanium (Ti) plate and deionized water ($H_2O$), which were obtained from Baoji Jinsheng Metal Material Co. Ltd and OneMed, respectively.

**Preparation of $TiO_2$ nanotube (TNT).** The synthesis of the $TiO_2$ nanotube was conducted by the anodization method. The titanium plate (4 cm × 1.5 cm × 0.02 cm, 0.3 mm thick, 99.6% purity) was cleaned via sanding using abrasive paper to remove impurities. Subsequently, the plate was sonicated in acetone and ethanol solutions at room temperature for 16 min each. The sonicated plate was then rinsed with deionized water and air dried. Anodization experiments were performed in an electrochemical cell comprising two electrodes (Ti plate and stainless steel as anode and cathode, respectively) with a potential of 40 V for 45 min. The electrolyte used was ethylene glycol, which contains 0.3% $NH_4F$ and 2% $H_2O$. The distance between the electrodes is 1.5 cm. The sample was then rinsed with deionized water, air dried, and calcined at 450 °C for 2 h to obtain the anatase phase from amorphous [15].

**Preparation of $BiFeO_3$/$TiO_2$ nanotube ($BiFeO_3$/TNT).** $BiFeO_3$/$TiO_2$ nanotube was synthesized by three deposition methods, namely SILAR, ultrasonication-assisted SILAR, and ultrasonic–immersion. The $BiFeO_3$/TNT prepared by the SILAR, ultrasonic-assisted SILAR, and ultrasonic immersion methods are symbolized as S, US, and UI, respectively. The first deposition technique, namely the SILAR method, was conducted by alternately immersing the TNT in 50 mL ethylene glycol containing 0.01 M $Bi(NO_3)_3$ solution and 0.01 M $Fe(NO_3)_3$ in 50 mL deionized water solution for 1 min each. Before each immersion, the sample was rinsed with ethanol and dried in the open air [12]. The immersion was repeated for several cycles to increase the $BiFeO_3$ loading ($BiFeO_3$/TNT_Sx, where x = a number of SILAR cycles). The same technique was used for US deposition but with the help of ultrasonication ($BiFeO_3$/TNT_USx). The third technique, namely the ultrasonic–immersion process, was performed first by creating a mixed solution of 0.808 g $Fe(NO_3)_3.9H_2O$ and 0.970 g $Bi(NO_3)_3.5H_2O$ dissolved in 20 mL ethylene glycol. Next, 20 µL of 0.1 M $HNO_3$, 0.42 g of citric acid, and 10 mL of ethylene glycol were added with stirring for 1 h at 60 °C. The sample was immersed in the solution for 1 h, accompanied by an ultrasonication process ($BiFeO_3$/TNT_UIx). The sample was then dried at 150 °C for 10 min. Furthermore, all synthesized $BiFeO_3$/TNT were calcined at 500 °C for 2 h [16].

**Characterization.** The optical properties of the samples were characterized by Fourier transform infrared (FTIR) and UV-Visible diffuse reflectance spectroscopic (UV-Vis DRS). A scanning electron microscopy-equipped energy-dispersive X-ray (SEM-EDX) was used to confirm the morphology and atomic composition of the samples, while the X-ray diffraction (XRD) spectrometer confirmed the crystal phase.

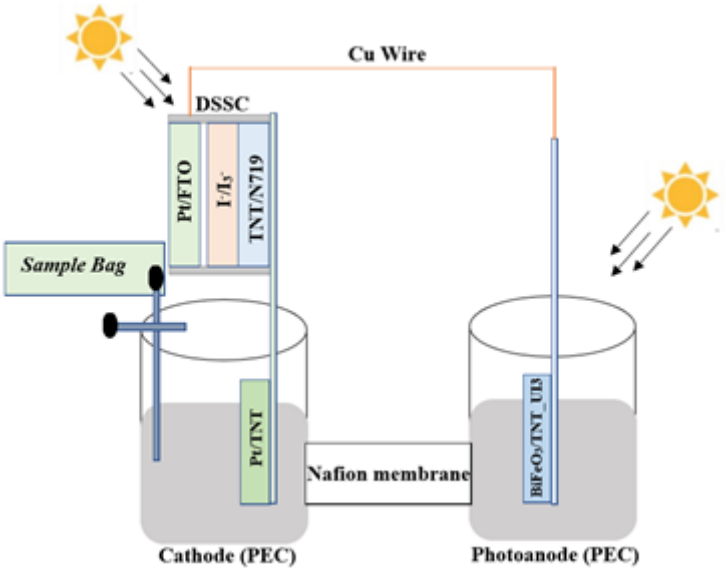


**Figure 1. Schematic of DSSC–PEC Preparation for Hydrogen Production**

**Photoelectrochemical test and evolution of hydrogen gas ($H_2$).** The synthesized $BiFeO_3$/TNT was tested photoelectrochemically using linear sweep voltammetry (LSV) and multiple-pulsed amperometry (MPA). Measurements with the LSV and MPA methods were conducted in $Na_2SO_4$ 0.1 M electrolyte with a three-electrode system, where $BiFeO_3$/TNT is the working electrode, Pt is the counter electrode, and Ag/AgCl is the reference electrode. This measurement uses visible light that comes from a white LED lamp with a power of 13 W. The evolution of hydrogen ($H_2$) gas was realized using a tandem system between DSSC and PEC cells. The arrangement of the DSSC cells follows a sandwich cell configuration. DSSC cells comprised TNT/N719 as an anode, $I^-/I_3^-$ as an electrolyte, and Pt/Fluorine-doped tin oxide (Pt/FTO) as a cathode. The synthesis of TNT/N719 was conducted by immersing TNT in a dye solution of N719 using 0.3 mM ethanol solvent at room temperature for 24 h [17]. The electrolyte solution $I^-/I_3^-$ was prepared by dissolving 0.13 g $I_2$ crystals in a mixed solvent of 20 mL acetonitrile and 5 mL ethylene glycol and then adding 0.18 g of KI powder and stirring for 30 min [18]. Pt/FTO electrode was prepared first by cleaning the FTO glass using sonication in pure ethanol. Next, drops of 40 mM $H_2PtCl_6$ in ethanol solution were added to its conductive surface before being heat-treated at 380 °C for 30 min [14]. The assembly and hydrogen evolution test of the DSSC–PEC system is illustrated in Figure 1. The process was conducted in two compartments of the H-reactor, namely the PEC cathode (Pt/TNT) and the PEC photoanode ($BiFeO_3$/TNT_UI3) connected by a Nafion membrane. The electrolyte used in both compartments was 50 mL of 0.5 M $H_2SO_4$. The DSSC anode part (TNT/N719) was connected to the PEC cathode and the DSSC cathode (Pt/FTO) part was connected to the PEC photoanode by Cu wire. A 400 W halide lamp was used as the visible light source in this experiment. This DSSC–PEC tandem system is connected to a sample bag to accommodate the $H_2$ gas production. The resulting $H_2$ gas was analyzed using gas chromatography with a thermal conductivity detector (GC-TCD) using an activated carbon column.

## Results and Discussions

The synthesis of $BiFeO_3$/TNT was conducted using the SILAR method and ultrasonic–immersion. The SILAR method aims to produce uniform and controlled particle growth. The principle of the SILAR method is based on the successive process between adsorption and reactions of two separate reactants to form a particle that could grow directly on the substrate [19]. One cycle of SILAR is completed when TNT has been successively immersed in $Bi^{3+}$ solution, rinsed with ethanol, immersed in $Fe^{3+}$ solution, and rinsed with ethanol again. The immersion of the sample in ethanol before each reactant was performed to decrease the adsorbed ions on the TNT, thus allowing slow and controllable particle growth. The possible reactions are as follows.

$$Bi^{3+} + 3OH^- \rightarrow Bi(OH)_3$$
$$Fe^{3+} + 3OH^- \rightarrow Fe(OH)_3$$
$$Bi(OH)_3 + Fe(OH)_3 \xrightarrow{\text{Calcination 500°C}} BiFeO_3 + 3H_2O$$

The ultrasonic–immersion method was conducted by immersing the TNT in a mixture of $Bi(NO_3)_3$ and $Fe(NO_3)_3$ in ethylene glycol at 60 °C. This process results in the formation of hydroxides, namely $Bi(OH)_3$ and $Fe(OH)_3$. The formation of $BiFeO_3$ occurred during the calcination process for both methods. The possible reactions are as follows.

$$Bi(NO_3)_3 + C_2H_6O_2 \rightarrow [Bi(C_2H_5O_2)]^{2+} + 3NO_3^- + H^+$$
$$Fe(NO_3)_3.9H_2O \rightarrow [Fe(H_2O)_9]^{3+} + 3NO_3^-$$
$$[Bi(C_2H_5O_2)]^{2+} + [Fe(H_2O)_9]^{3+} \rightarrow C_2H_6O_2 + Bi(OH)_3 + Fe(OH)_3 + 11H^+ + 3O^-$$
$$Bi(OH)_3 + Fe(OH)_3 \xrightarrow{\text{Calcination } 500^\circ C} BiFeO_3 + 3H_2O$$

UV-Vis DRS characterization aimed to determine the band gap energy of $TiO_2$ nanotube and $BiFeO_3/TiO_2$ nanotube (TNT and $BiFeO_3$/TNT). The results of the UV-Vis DRS characterization of TNT and $BiFeO_3$/TNT synthesized using the SILAR method, ultrasonication-assisted SILAR method, and ultrasonic–immersion method with three cycles can be seen in Figure 2(a). Similar to the well-known anatase phase (3.20 eV), the synthesized TNT has a band gap of 3.21 eV [7]. The synthesized $BiFeO_3$/TNT had a band gap of 2.81, 2.63, and 2.69 eV for $BiFeO_3$/TNT_S3, $BiFeO_3$/TNT_US3, and $BiFeO_3$/TNT_UI3, respectively. Band gap values were obtained using the Kubelka–Munk and Tauc equations [20]. Fu *et al.* stated that the $BiFeO_3$ band gap value is 2.0–2.8 eV [8]. These data indicate that the $BiFeO_3$ deposited on TNT succeeded in reducing the band gap value, thus increasing its activity in the visible region. The lower band gap of $BiFeO_3$/TNT_US3 compared with other techniques indicates that the sonication process affects the deposition of $BiFeO_3$ on TNT. Additional deposits of $BiFeO_3$ on TNT can reduce the bandgap. In addition, the size of the $BiFeO_3$ affects the band gap.

The FTIR spectra of TNT and $BiFeO_3$/TNT measured from the wavenumber of 4000–400 $cm^{-1}$ are shown in Figure 2(b). Ti-O-Ti bonds at a wavenumber of 900–450 $cm^{-1}$ centered at 833 $cm^{-1}$. Furthermore, a bending -OH group at wavenumber 1800–1400 $cm^{-1}$ and -OH group stretching at wavenumber 3600–3000 $cm^{-1}$ are observed. This -OH group indicates the presence of a TNT surface that is still attached to water molecules. In the spectrum of $BiFeO_3$/TNT_S3 and $BiFeO_3$/TNT_US3, an additional peak is observed at the wavenumber of 439 $cm^{-1}$, which is a bending O-Fe-O group [21]. When $BiFeO_3$ was deposited with TNT using the SILAR method, the release of Bi ions occurred during washing with ethanol. However, in the $BiFeO_3$/TNT_UI3, two additional groups at a wave number of 439 $cm^{-1}$, namely O-Fe-O bending and Fe-O stretching, appeared at a wavenumber of 545 $cm^{-1}$. These results are similar to the previous report, which states that those peaks belong to the octahedral group of $FeO_6$ perovskite [21, 22].

Figure 3(a) shows the results of the LSV test on $BiFeO_3$/TNT samples with various methods when exposed to visible light with a 13 W white LED lamp. The electrolyte solution was in a 0.1 M $Na_2SO_4$ solution. The current in the LSV was measured from potential −1 to 1 V with a scan rate of 25 mV/s. Based on the figure, the current density of $BiFeO_3$/TNT_UI3 is higher than the others. $BiFeO_3$/TNT using the SILAR method, the ultrasonication-assisted SILAR method, and the ultrasonic–immersion method with three cycles were also analyzed using the MPA method to determine the current response to visible light without being given a voltage. This measurement was conducted at a potential of 0 V with a visible light irradiation time every 10 s using 13 W white LED lamp. Figure 3(b) shows the following: when visible light is applied, the current density increases sharply; when the visible light is turned off, the current density decreases sharply. The LSV and MPA data reveal that the current density of produced TNT is remarkably small when exposed to visible light. However, when deposited with $BiFeO_3$, the current density increased, which is incorporated into the increase in the photocatalytic activity. This phenomenon can be due to the incorporation of the small band gap material and the

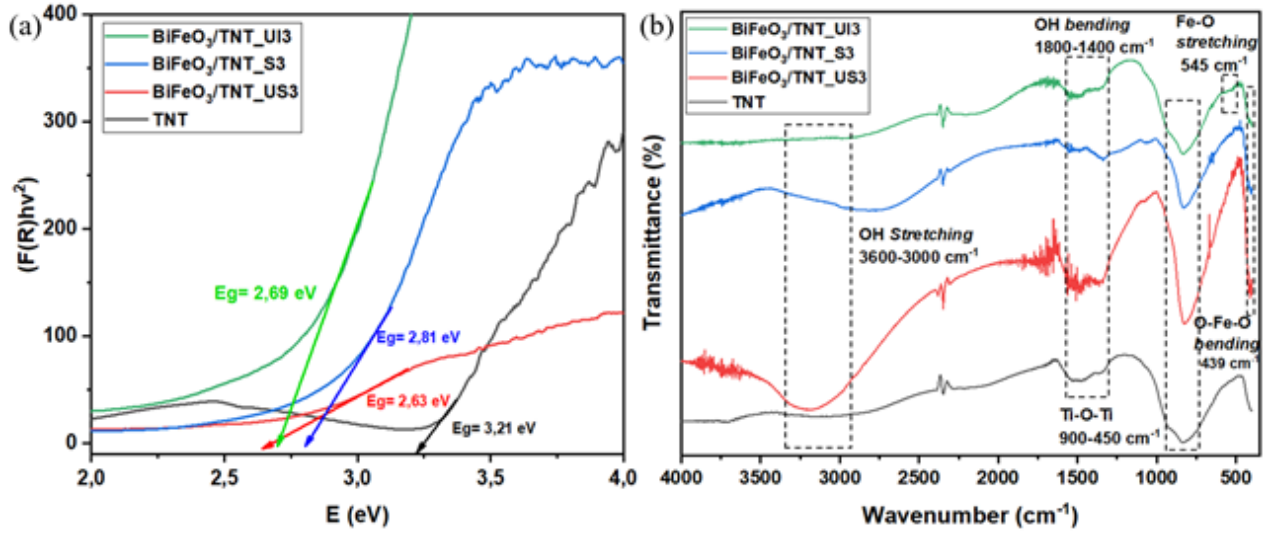


**Figure 2. (a) Curve of the Bandgap Values using Kubelka–Munk and Tauc Calculations; (b) FTIR Spectra of TNT and $BiFeO_3$/TNT at Three Cycles**

suitable junction of band energy between $BiFeO_3$ and TNT [23]. The principle that occurs is as follows: when $BiFeO_3$/TNT is given sufficient energy or larger than its band gap energy, the electron excitation process occurs toward the conduction band from the valence band. The resulting electrons are measured as the current density. Of the three methods, the current density produced using the ultrasonic–immersion method is higher than the others by up to 0.009 mA/cm$^2$. This finding indicates the excitation of additional electrons due to the small bandgap, thus increasing the current density when exposed to visible light. A small band gap indicates a high current density. The band gap value is influenced by the morphology or the size of the $BiFeO_3$. In the ultrasonic–immersion method, $BiFeO_3$ was effectively deposited on TNT, resulting in fast charge transfer and slow recombination, which shows an increase in photoelectrochemical properties compared with $BiFeO_3$/TNT synthesized using the SILAR method because $BiFeO_3$ was ineffectively deposited. Ferroelectricity can induce electrical polarization when deposited with $BiFeO_3$ [24]. Thus, $BiFeO_3$/TNT has high efficiency in charge separation by visible light.

The $BiFeO_3$/TNT synthesis was then continued in cycles to achieve optimum results for each method. The SILAR, ultrasonication-assisted SILAR, and ultrasonic–immersion methods obtained optimum results at 15, 5, and 3 cycles, respectively. In the SILAR method, additional cycles are needed to achieve optimum results. This condition is attributed to the accelerated penetration of the ions $Fe^{3+}$ and $Bi^{3+}$ in the TNT due to sonication. These optimum cycles were characterized by UV-Vis DRS, FTIR, potentiostat, XRD, and SEM-EDX.

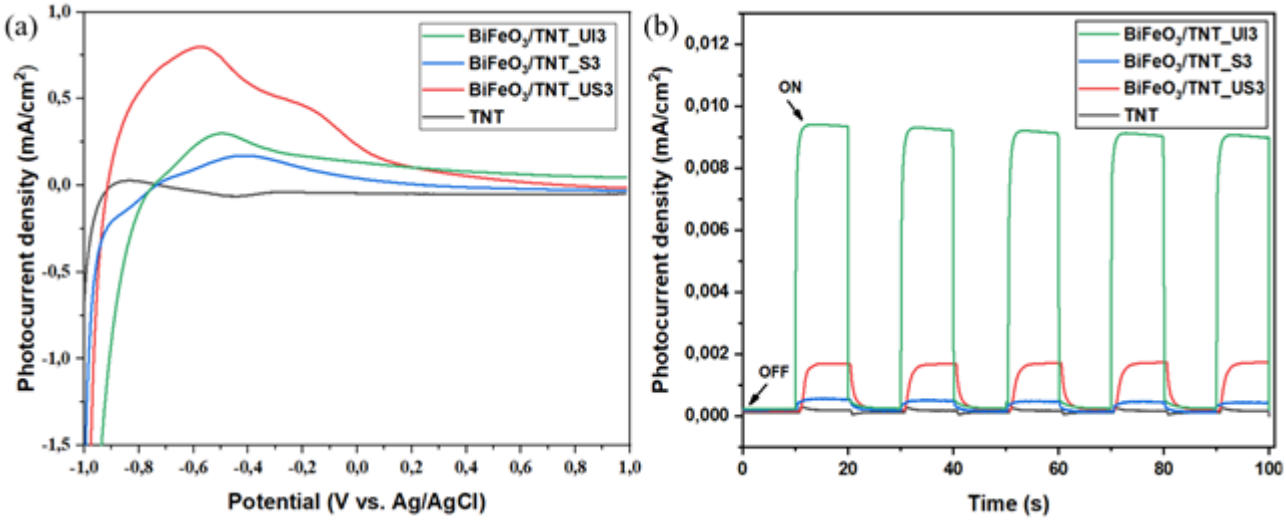


**Figure 3. (a) LSV and (b) MPA of TNT and $BiFeO_3$/TNT at Three Cycles**

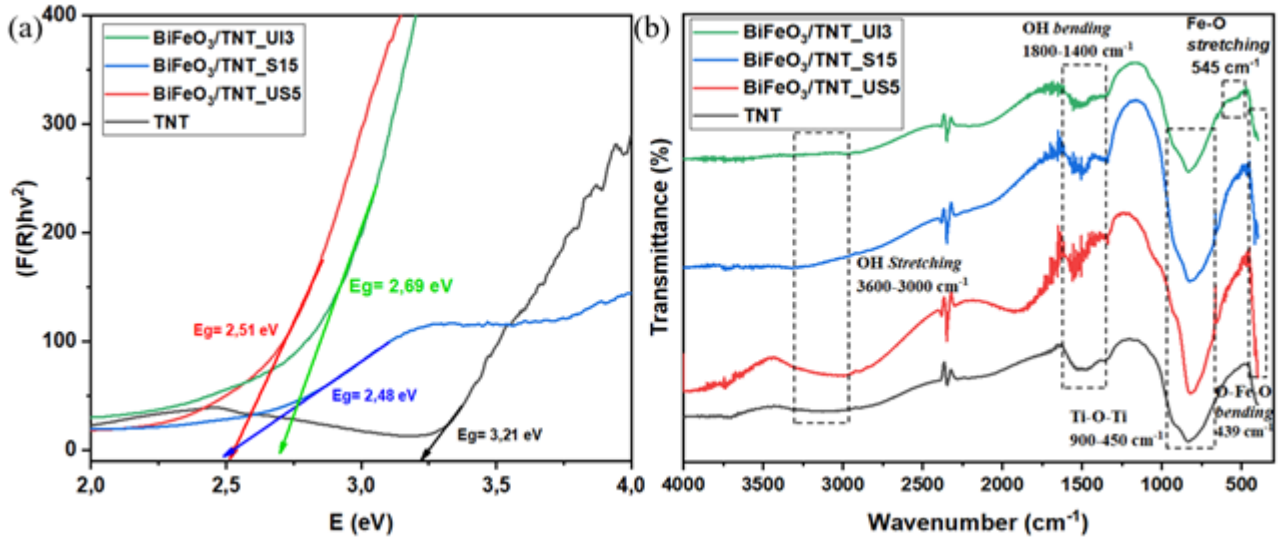


**Figure 4. (a) Curve of the Band Gap Values using Kubelka–Munk and Tauc Calculations; (b) FTIR Spectra of TNT and $BiFeO_3$/TNT at Optimum Cycle**

The results of the UV-Vis DRS characterization of TNT and $BiFeO_3$/TNT synthesized using the SILAR method, ultrasonication-assisted SILAR method, and ultrasonic–immersion method are shown in Figure 4(a). The synthesized $BiFeO_3$/TNT had band gaps of 2.51, 2.48, and 2.69 eV for $BiFeO_3$/TNT_US5, $BiFeO_3$/TNT_S15, and $BiFeO_3$/TNT_UI3, respectively. In the condition of $BiFeO_3$/TNT junction, the low band gap result might be attributed to the high amount of deposited $BiFeO_3$ on the TNT. The difference in the number of cycles in each technique to achieve almost similar bandgap shows the different kinetics of particle growth of each deposition technique.

Figure 4(b) shows the FTIR spectra of TNT and $BiFeO_3$/TNT measured from wavenumbers 4000–400 $cm^{-1}$ using the SILAR method with 5 cycles of ultrasonication, the ultrasonication-assisted SILAR method with 15 cycles, and the ultrasonic–immersion method with 3 cycles. The resulting FTIR characterization is the same as in Figure 2(b), thereby demonstrating the presence of Ti-O-Ti bonds, -OH bending, and -OH stretching groups. O-Fe-O bending and Fe-O stretching groups are observed in the spectrum of $BiFeO_3$/TNT synthesized using the ultrasonic–immersion method.

The XRD characterization of TNT and $BiFeO_3$/TNT is shown in Figure 5, and the diffraction pattern of TNT reveals the presence of crystal peaks of $TiO_2$ anatase and metal titanium. The crystal peak of $TiO_2$ anatase is 2Θ at 25.37° (101), 37.96° (004), 48.10° (200), 53.97° (105), 55.02° (211), 63.01° (204), and 76.26° (301), which has been adjusted with ICDD NO. 01-089-4921. In addition to the $TiO_2$ peak, the Titanium (Ti) peak was found at an angle of 2Θ, namely 35.15° (100), 38.50° (002), 40.23° (101), 53.08° (102), 70.70° (103), 77.27 (201), and 82.33° (004), which has been adjusted to the ICDD NO. 00-044-1294. The $BiFeO_3$/TNT_UI3 diffraction pattern shows two additional peaks, namely $BiFeO_3$ crystal peaks from the planes (104) and (110), which are perovskite structures that have been adjusted in accordance with ICDD NO. 01-077-8326.

Figure 6(a) shows that the current density of $BiFeO_3$/TNT_UI3 is higher than that of the others. The $BiFeO_3$ is evenly deposited on the TNT. Therefore, when irradiated with visible light, the electron excitation process occurs toward the conduction band from the valence band, resulting in high current density. $BiFeO_3$/TNT synthesized at the optimum cycle was also analyzed using the MPA method. Figure 6(b) shows that the current density generated using the ultrasonic–immersion method is higher than the others by up to 0.009 $mA/cm^2$. This finding indicates that more electrons are generated compared with other samples because the current density increases when exposed to visible light.

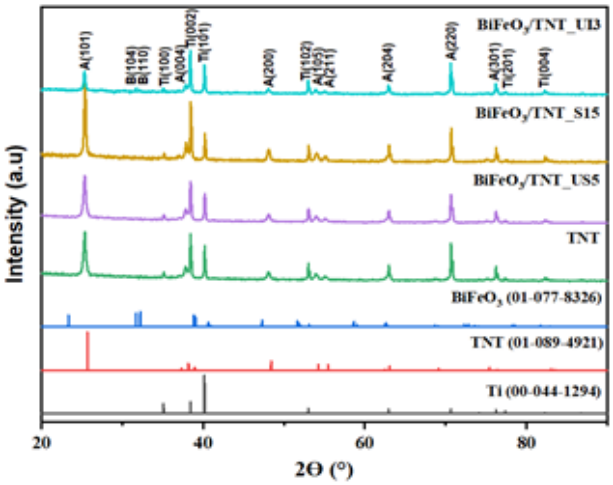


**Figure 5. XRD Diffractograms of TNT and $BiFeO_3$/TNT at Optimum Cycles**

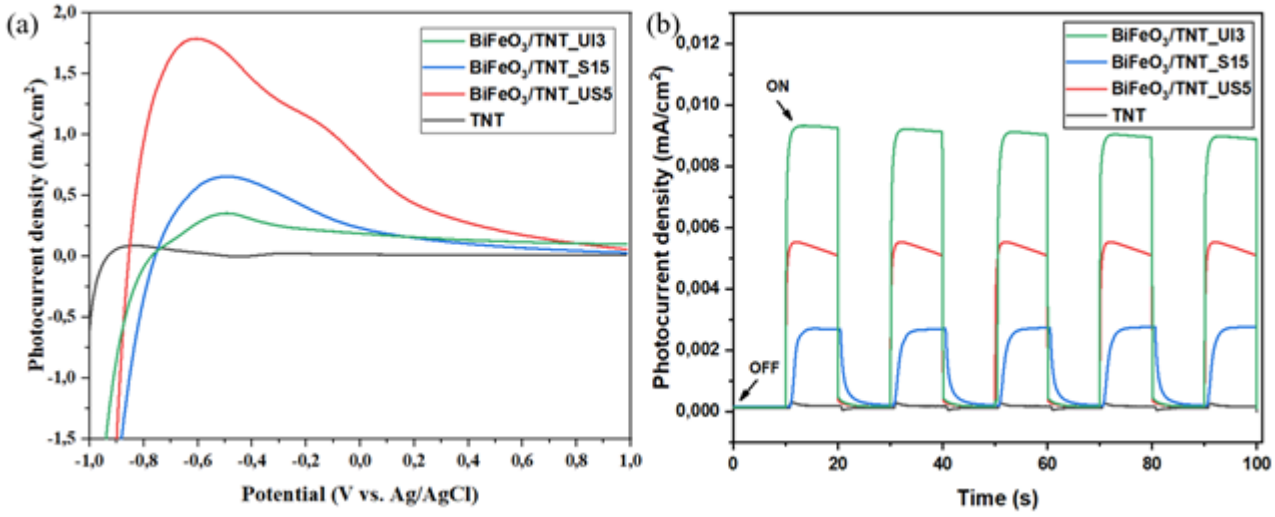


**Figure 6. (a) LSV and (b) MPA TNT and $BiFeO_3$/TNT at Optimum Cycle**

Figure 7(a) depicts the SEM image of the obtained TNT sample, which shows the form of nanotubes arranged in an orderly manner. The top morphology of the $BiFeO_3$/TNT_UI3 sample as the best-obtained photoelectrode is shown in Figure 7(b). The $BiFeO_3$ was observed around the edge of the TNT wall with white color without covering the nanotube holes. These observations indicate that this deposition process does not damage the nanotube structure in TNT. This result is also supported by EDX, which shows that the percentage of constituent elements in the synthesized $BiFeO_3$/TNT_UI3 sample contained elements of Ti, O, Bi, and Fe, which is shown in Figure 7(c). The EDX data of the $BiFeO_3$/TNT_UI3 show that the percentage ratio by weight of Ti:O:Bi:Fe is 55.92: 39.66: 3.20: 1.21, with the atomic ratio of Bi and Fe to 0.7:1. This EDX result confirmed that $BiFeO_3$ had been deposited on TNT.

Next, the efficiency of the DSSC, which is used in the tandem system, was measured**.** Figure 8 shows the I–V curve of the DSSC when exposed to visible light using a 13 W white LED lamp. This measurement is conducted using the LSV method with a potential range of 0 to 1 V. The figure reveals that the values of short-circuit photocurrent (Jsc), open-circuit photocurrent (Voc), maximum current (Jmax), maximum voltage (Vmax), maximum power point (Pmax), fill factor (FF), and efficiency (η) were determined and are shown in Table 1. DSSC efficiency can be calculated using Equation 1 [25]:

$$\%\eta = \frac{FF \times Voc \times Jsc}{Pin} x\ 100\%. \quad (1)$$

Based on Equation 1, the DSSC efficiency value is 1.27% and the efficiency value increases with the Jsc and Voc values. A high value of Jsc indicates a reduction in electron recombination. The FF value obtained was 0.304. The FF is a parameter that measures solar cell quality and maximum power. The DSSC used herein can help the system achieve unbiased hydrogen evolution from water despite its lower efficiency and FF value compared with other results. This DSSC aims to produce additional electrons that enter the catalysis zone to increase the amount of hydrogen formed using the water splitting process.

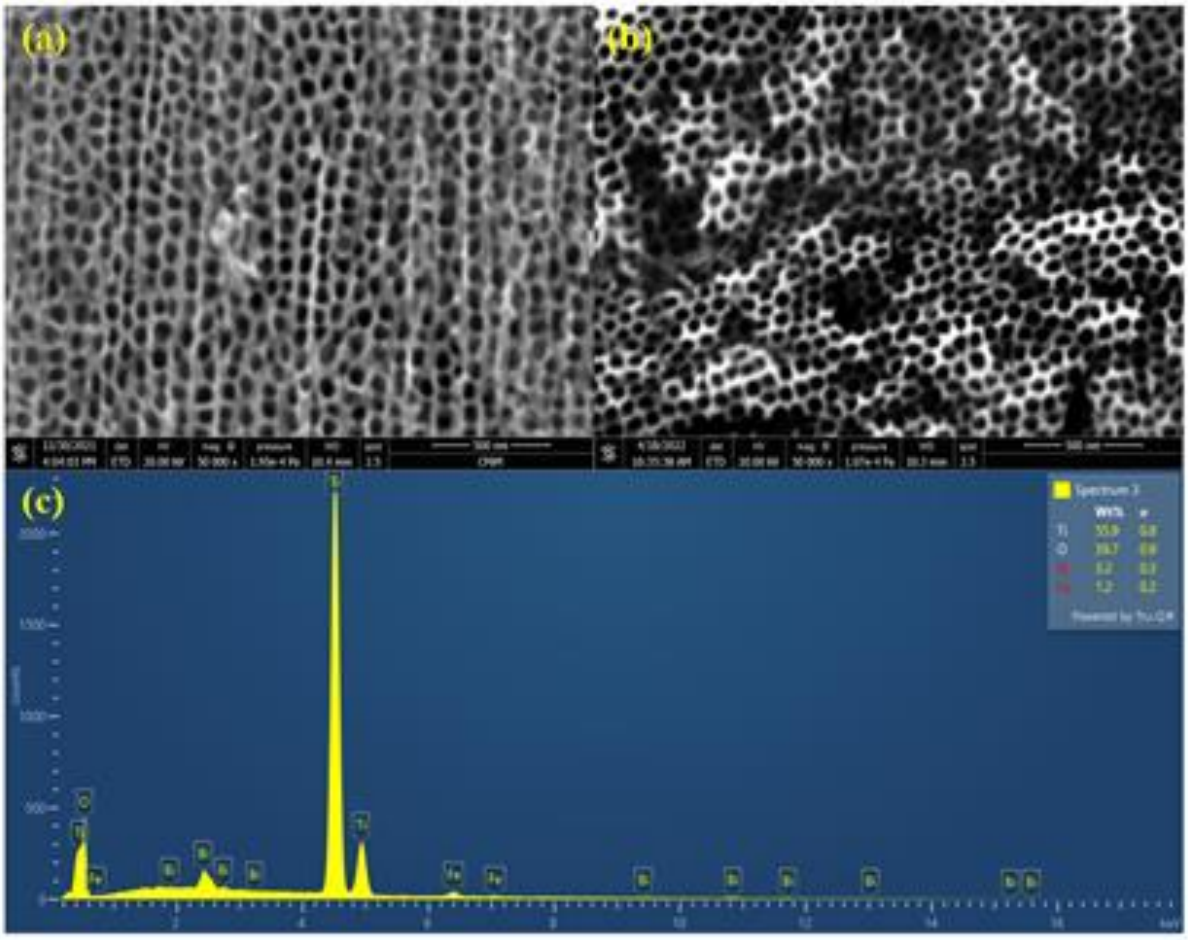


**Figure 7. Surface Morphology by SEM (a) TNT with a Magnification of 50,000x; (b) $BiFeO_3$/TNT with Three Cycles of Ultrasonic–immersion Method with a Magnification of 50,000x; (c) EDX $BiFeO_3$/TNT with Three Cycles of Ultrasonic–immersion Method**

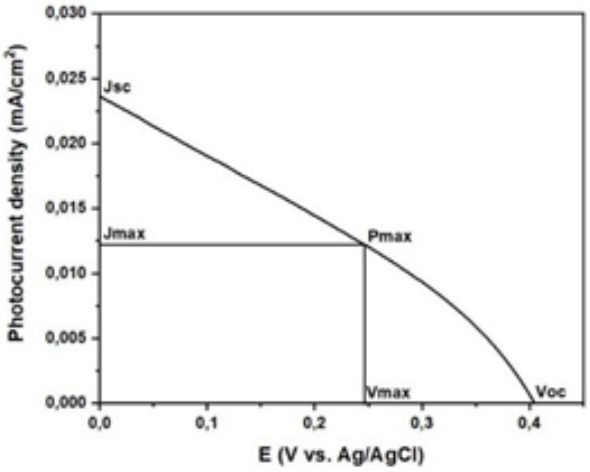


**Figure 8. I–V Curve to Measure the Efficiency of DSSC**

**Table 1. Photovoltaic Performance on DSSC Arranged with a Sandwich Structure**

| Jsc ($mA/cm^2$) | Voc (V) | Max ($mA/cm^2$) | Vmax (V) | Max ($mW/cm^2$) | Pin ($mW/cm^2$) | FF | %η |
|---|---|---|---|---|---|---|---|
| 0.024 | 0.404 | 0.012 | 0.246 | 0.003 | 0.237 | 0.304 | 1.27% |

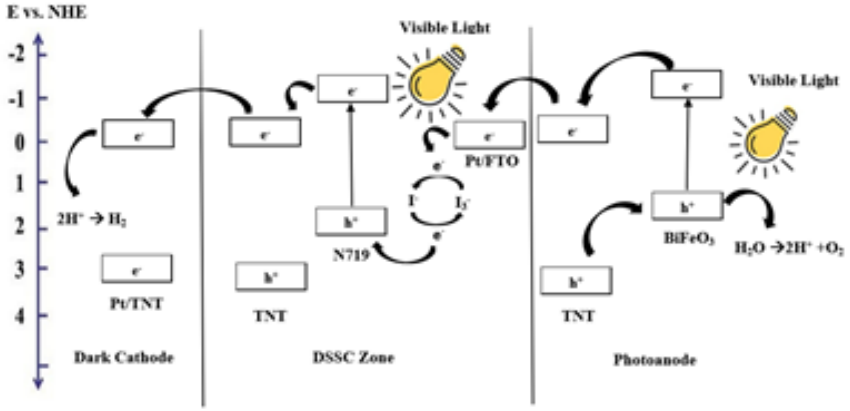


**Figure 9. Schematic Illustration of the Hydrogen Evolution Mechanism**

Afterward, the DSSC–PEC tandem system was constructed, as shown in Figure 1. In the DSSC part, there was Pt/FTO as cathode and TNT/N719 as anode using electrolyte solution from $I^-/I_3^-$ while the PEC part used $BiFeO_3$/TNT_UI3 which was synthesized at photoanode and Pt/TNT at the dark cathode where $H_2$ is generated. Hydrogen production was conducted for 6 h in an H-reactor filled with $H_2SO_4$ 0.5 M with a photoanode, DSSC (cross-sectional area of each 3 $cm^2$) was irradiated by a 400 W metal halide lamp (equivalent with 3.588 $mW/cm^2$), the cathode was left in the dark. The $H_2$ gas formed was then captured in a sample bag and analyzed using GC-TCD. The solar-to-hydrogen (STH) efficiency was calculated using Equation 2.

$$\eta = \frac{[r_{H2}]\Delta G}{PA}. \quad (2)$$

The obtained STH efficiency was 0.0033% from this experiment. The experiment was also performed under dark conditions without any illumination. The analysis using GC-TCD revealed the absence of $H_2$ gas in the dark condition, indicating the need for a light source to run the system. The energy source for the excitation of electrons is insufficient in the absence of light, leaving holes to oxidize water and electrons to reduce $H^+$ to $H_2$.

The reaction mechanism for hydrogen evolution in the DSSC–PEC tandem system is illustrated in Figure 9; that is, when exposed to visible light, light absorption occurs

at the DSSC and $BiFeO_3$/TNT_UI3 photoanode. In the DSSC section, the dye N719 in TNT/N719 experiences electron excitation ($e^-$) from HOMO N719 to LUMO N719 when exposed to light, leaving a hole ($h^+$) in the HOMO. The electrons ($e^-$) then flow into the TNT conduction band and toward the Ti plate. Furthermore, electrons ($e^-$) flow into the external circuit to the PEC cathode. These electrons play a role in reducing $H^+$ to $H_2$. Meanwhile, at the photoanode, the electrons ($e^-$) are excited from the valence band (VB) to the conduction band of the $BiFeO_3$, then leaving a hole ($h^+$) in the VB. Next, the electrons ($e^-$) proceed to the Pt/FTO (DSSC cathode) through the external circuit to regenerate the electrolyte ($I^-/I_3^-$). The resulting hole ($h^+$) oxidizes water into $O_2$ while generating protons ($H^+$). The $H^+$ produced then moves from the photoanode to the PEC cathode (Pt/TNT) through the Nafion membrane [25].

## Conclusions

$BiFeO_3$/TNT was synthesized using SILAR, ultrasonication-assisted SILAR, and ultrasonic–immersion methods with optimum cycles of 15, 5, and 3, respectively. The synthesized $BiFeO_3$/TNT produces a small band gap value and extends its activity toward visible light. The current densities generated from $BiFeO_3$/TNT_S15, $BiFeO_3$/TNT_US5, and $BiFeO_3$/TNT_UI3 are 0.003, 0.005, and 0.009 mA/cm$^2$, respectively. $BiFeO_3$ plays an important role in charge separation under visible light, where the highest current density at MPA is 0.009 mA/cm$^2$ and is synthesized by the ultrasonic–immersion method. The efficiency of solar cells on the DSSC from the DSSC–PEC tandem system was 1.27%, while the DSSC–PEC tandem system for producing $H_2$ with dark cathode and anode conditions and DSSC irradiated with visible light obtained STH efficiency of 0.0033%. Hydrogen production was absent under dark conditions at both the cathode, anode, and DSSC.

## Acknowledgments

The authors gratefully acknowledge the support from DGHE, Directorate General of Higher Education, for funding the research (PDUPT research contract No. NKB-174/UN2.RST/HKP.05.00/2021).

## References

[1] Rosen, M.A., Koohi-Fayegh, S. 2016. The Prospects for Hydrogen as An Energy Carrier: An Overview of Hydrogen Energy and Hydrogen Energy Systems. Energy Ecol. Environ. 1(1): 10–29, https://doi.org/10.1007/s40974-016-0005-z.

[2] Rohendi, D., Rahmah, D.R., Yulianti, D.W., Amelia, I., Sya'baniah, N.F., Syarif, N., Rachmat, A. 2018. A Review on Production of Hydrogen from Renewable Sources and Applications for Fuel Cell Vehicles. Int. J. Sustain. Transp. Technol. 1(2): 63–68, https://doi.org/10.31427/ijstt.2018.1.2.5.

[3] Ahmed, M., Dincer, I. 2019. A Review on Photoelectrochemical Hydrogen Production Systems: Challenges and Future Directions. Int. J. Hydrog. Energy. 44(5): 2474–2507, https://doi.org/10.1016/j.ijhydene.2018.12.037.

[4] Wu, H.S., Lesmana, D. 2012. Short review: Cu Catalyst for Autothermal Reforming Methanol for Hydrogen Production. Bull. Chem. React. Eng. Catal. 7(1): 27–42, https://doi.org/10.9767/bcrec.7.1.1284.27-42.

[5] Nazemzadegan, M., Ghasempour, R. 2019. Evaluating The Materials Used for Hydrogen Production Based on Photoelectrochemical Technology. Int. J. Renew. Energy Dev. 8(2): 169–178, https://doi.org/10.14710/ijred.8.2.169-178.

[6] Fujishima, A., Honda, K. 1972. Electrochemical Photolysis of Water at a Semiconductor Electrode. Nature. 238(5358): 38–40, https://doi.org/10.1038/238038a0.

[7] Ola, O., Maroto-Valer, M.M. 2015. Review of Material Design and Reactor Engineering on TiO2 Photocatalysis for $CO_2$ Reduction. J. Photochem. Photobiol. C Photochem. Rev. 24: 16–4, https://doi.org/10.1016/j.jphotochemrev.2015.06.001.

[8] Fu, Y., Mao, Z., Zhou, D., Hu, Z., Tu, Y., Tian, Y., Zhu, X., Zheng, G. 2019. Preparation of BiFeO3-Overcoated TiO2 Nanorod Arrays For The Enhanced Visible-Light Activity. Mater. Res. Expr. 6(10): 1–9, https://doi.org/10.1088/2053-1591/ab41 b6.

[9] Owolabi, T.O., Rahman, M.A.A. 2021. Energy Band Gap Modeling of Doped Bismuth Ferrite Multifunctional Material Using Gravitational Search Algorithm Optimized Support Vector Regression. Crystals. 11(3): 1–15, https://doi.org/10.3390/cryst11030246.

[10] Liao, X., Li, T., Ren, H., Mao, Z., Zhang, X., Lin, J., Lou, C. 2021. Enhanced Photocatalytic Performance Through The Ferroelectric Synergistic Effect of p-n Heterojunction $BiFeO_3/TiO_2$ Under Visible-Light Irradiation. Ceram. Int. 47(8): 10786–10795, https://doi.org/10.1016/j.ceramint.2020.12.195.

[11] Wu , X., Li, H., Wang, X., Jiang, L., Xi, J., Du, G., Ji, Z. 2019. Ferroelectric Enhanced Photoelectrochemical Water Splitting in $BiFeO_3/TiO_2$ Composite Photoanode. J. Alloys Compd. 783: 643–651, https://doi.org/10.1016/j.jallcom.2018.12.345.

[12] Zhao, Q., Ren, Y., Li, X., Shi, Y. 2016. Photo-induced activity of $BiFeO_3/TiO_2$ Nanotube Arrays Derived From Ultrasound-Assisted Successive Ionic Layer Adsorption and Reaction. Mater. Res. Bull. 83: 396–399, https://doi.org/10.1016/j.materresbull.2016.06.031.

[13] Samsudin, M.F.R., Sufian, S., Mohamed, N.M., Bashiri, R., Wolfe, F., Ramli, R.M. 2018. Enhancement of Hydrogen Production Over Screen-

Printed $TiO_2/BiVO_4$ Thin Film in The Photoelectrochemical Cells. Mater. Lett. 211: 13-16, https://doi.org/10.1016/j.matlet.2017.09.013.

[14] Surahman, H. 2017. Pengembangan Sel Fotoelektrokimia Menggunakan Elektroda $TiO_2$ Nanotube Arrays Tersensitasi CdS Nanopartikel Untuk Produksi Hidrogen [Disertasi]. Departemen Kimia: Universitas Indonesia.

[15] Surahman, H., Supriyono, Krisnandi, Y.K., Gunlazuardi, J. 2015. Modification of Mixed Structure $TiO_2$ Nanoporous-Nanotube Arrays with CdS Nanoparticle and Their Photoelectrochemical Properties. J. Sains Mater. Indones. 16(3): 118–125, https://doi.org/10.17146/jsmi.2015.16.3.4229.

[16] Zhu, A., Zhao, Q., Li, X., Shi, Y. 2014. $BiFeO_3/TiO_2$ Nanotube Arrays Composite Electrode: Construction, Characterization, and Enhanced Photoelectrochemical Properties. ACS Appl. Mater. Interfaces. 6: 671–679, https://doi.org/10.1021/am404774z.

[17] Ramakrishnan, V.M., Pitchaiya, S., Muthukumarasamy, N., Kvamme, K., Rajesh, G., Agilan, S., Pugazhendhi, A., Velauthapillai, D. 2020. Performance of $TiO_2$ Nanoparticles Synthesized by Microwave and Solvothermal Methods as Photoanode in Dye-Sensitized Solar Cells (DSSC). Int. J. Hydrog. Energy. 45(51): 27036–27046, https://doi.org/10.1016/j.ijhydene.2020.07.018.

[18] Gu, P., Yang, D., Zhu, X., Sun, H., Wangyang, P., Li, J., Tian, H. 2017. Influence of Electrolyte Proportion on The Performance of Dye-Sensitized Solar Cells. AIP Adv. 7(10): 1–9, https://doi.org/10.1063/1.5000564.

[19] Kale, S.S., Mane, R.S., Chung, H., Yoon, M.Y., Lokhande, C.D., Han, S.H. 2006. Use of Successive Ionic Layer Adsorption and Reaction (SILAR) Method For Amorphous Titanium Dioxide Thin Films Growth. Appl. Surf. Sci. 253(2): 421–424, https://doi.org/10.1016/j.apsusc.2005.12.082.

[20] Makuła, P., Pacia, M., Macyk, W. 2018. How To Correctly Determine the Band Gap Energy of Modified Semiconductor Photocatalysts Based on UV-Vis Spectra. J. Phys. Chem. Lett. 9(23): 6814–6817, https://doi.org/10.1021/acs.jpclett.8b02892.

[21] Mohamed, M.M., Reda, S.M., Amer, A.A. 2020. Enhanced Performance of $BiFeO_3$@nitrogen Doped TiO2 Core-shell Structured Nanocomposites: Synergistic Effect Towards Solar Cell Amplification. Arab. J. Chem. 13(1): 2611–2619, https://doi.org/10.1016/j.arabjc.2018.06.013.

[22] Psathas, P., Solakidou, M., Mantzanis, A., Deligiannakis, Y. 2021. Flame Spray Pyrolysis Engineering of Nanosized Mullite-$Bi_2Fe_4O_9$ and Perovskite-$BiFeO_3$ as Highly Efficient Photocatalysts for $O_2$ Production from $H_2O$ Splitting. Energies. 14(5235): 1–16, https://doi.org/10.3390/en14175235.

[23] Yang, Y.C., Liu, Y., Wei, J.H., Pan, C.X., Xiong, R., Shi, J. 2014. Electrospun Nanofibers of p-type $BiFeO_3$/n-type $TiO_2$ Hetero-junctions with Enhanced Visible-Light Photocatalytic Activity. RSC Adv. 4(60): 31941–31947, https://doi.org/10.1039/c4ra04258a.

[24] Lee, H., Joo, H., Yoon, C., Lee, J., Lee, H., Choi, J., Park, B, Choi, T. 2017. Ferroelectric $BiFeO_3/TiO_2$ Nanotube Heterostructures for Enhanced Photoelectrochemical Performance. Curr. Appl. Phys. 17(5): 679–683, https://doi.org/10.1016/j.cap.2017.02.015.

[25] Francis, O.I., Ikenna, A. 2021. Review of Dye-Sensitized Solar Cell (DSSCs) Development. Nat. Sci. 13(12): 496–509, https://doi.org/10.4236/ns.2021.1312043.